BEHAVIOR OF FLOWING BODIES NEAR A BIFURCATION: ELUCIDATING THE ZWEIFACH-FUNG EFFECT

Vincent Doyeux, Thomas Podgorski, Sarah Peponas, Mourad Ismail, Gwennou Coupier

μFLU10-64

BEHAVIOR OF FLOWING BODIES NEAR A BIFURCATION: ELUCIDATING THE ZWEIFACH-FUNG EFFECT

Vincent Doyeux[1], Thomas Podgorski[1], Sarah Peponas[1], Mourad Ismail[1], Gwennou Coupier *[1]
[1]Laboratoire de Spectrométrie Physique, CNRS et Université J. Fourier - Grenoble I, BP 87, 38402 Saint-Martin d'Hères, France
vincent.doyeux@gmail.com, tpodgors@spectro.ujf-grenoble.fr,sarah.peponas@u-picardie.fr, ismail@spectro.ujf-grenoble.fr,gcoupier@spectro.ujf-grenoble.fr

KEY WORDS

Blood flow - Suspensions - Complex geometries

ABSTRACT

The problem of the splitting of a suspension in bifurcating channels dividing into two branches of non equal flow rates is addressed. As observed for long, in particular in blood flow studies, the volume fraction of particles generally increases in the high flow rate branch and decreases in the other one. We focus here on the possibility of an attraction of the particles towards one branch through microfluidic experiments and two-dimensional simulations and show that it is directed towards the low flow rate branch. The enrichment in particles in the high flow rate branch is shown to be mainly a consequence of the initial distribution in the inlet branch, which shows necessarily some depletion near the walls.

1. INTRODUCTION

When a suspension of particles reaches an asymmetric bifurcation, it is well-known that the particles volume fractions in the two daughter branches are not equal; basically, for branches of comparable geometrical characteristics, but receiving different flow rates, the volume fraction in particles increases in the high flow rate branch. This phenomenon, sometimes called Zweifach-Fung effect [1, 2], has been observed for long in the blood circulation. Under standard physiological circumstances, a branch receiving typically one fourth of the blood inflow will see its hematocrit (volume fraction of red blood cells) drop down to zero, which will have obvious physiological consequences.

Apart the huge number of in-vivo studies on blood flow (see ref. [3] for a review), many other papers have been devoted to this effect, either to understand it, or to use it in order to engineer sorting or purification devices. In the latter case, one can play at will with the different parameters characterizing the bifurcation (widths of the channels, relative angles of the branches), in order to reach a maximum of efficiency. As proposed in many papers, focusing on plain spheres can already give some keys to understand or control this phenomenon [4–11]. In-vitro behavior of red blood cells has also attracted some attention [10, 12–17].

All the latter papers consider the low-Reynolds-number limit, which is the relevant limit for applicative purposes and for the biological systems of interest. Therefore, this limit is also considered throughout this paper.

In most studies as well as in in vivo blood flow studies, which are for historical reasons the main sources of data, the main output is the particle volume fraction in the two daughter branches as a function of the flow

* Corresponding author

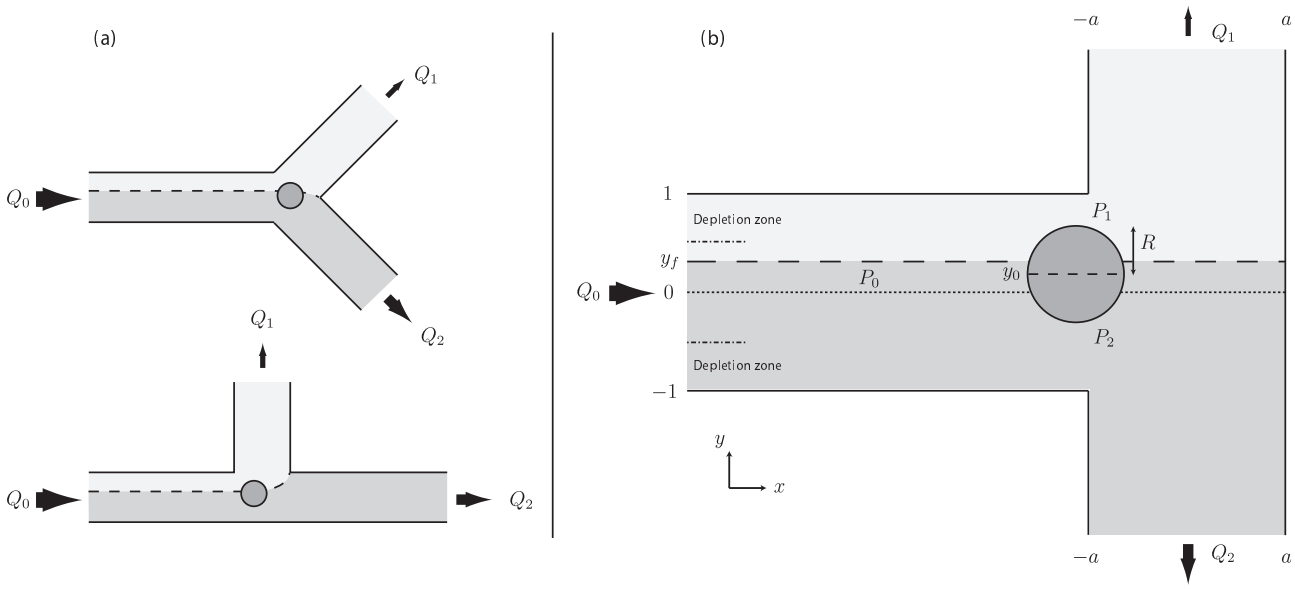

Figure 1: (a) The two Y-shaped geometries mainly studied in the literature. Here $Q_1 < Q_2$ and the dashed line stands for the separating streamline between the flows that will eventually enter branches 1 and 2 in the absence of particles. (b) The T-bifurcation that is studied in this paper and also in ref. [5] in order to get rid of geometrical effects as much as possible.

rate ratio between them. Such data can be well described by empirical laws that still depend on some ad-hoc parameters but allow some rough predictions [12,13,18], which have been exhaustively compared recently [19]. On the other hand, measuring macroscopic data such as volume fractions does not allow to identify the relevant parameters and effects involved in this asymmetric partitioning phenomenon.

For a given bifurcation geometry and a given flow rate ratio between the two outlet branches, the final distribution of the particles can be straightforwardly derived from two data: first, their spatial distribution in the inlet; second, their trajectories in the vicinity of the bifurcation, starting from all possible initial positions. If the particles follow their underlying unperturbed streamlines (as would a sphere do in a Stokes flow in a straight channel), their final distribution can be easily computed, although particles near the apex of the bifurcation require some specific treatment, since they cannot approach it as much as their underlying streamline does.
The relevant physical question in this problem is thus to identify the hydrodynamic phenomenon at the bifurcation that would make flowing objects escape from their underlying streamlines, which would have as a consequence that a large particle would be driven towards one branch while a tiny fluid particle located at the same position would go to the other branch.

The radial distribution in the inlet channel obviously plays a key role also: in an extreme case where all the particles are centered in the inlet channel and follow the underlying fluid streamline, they all enter in the high flow rate branch; more generally the existence of a free layer near the walls favours the high flow rate branch, since the depletion in particles it entails is relatively more important for the low flow rate branch, which receives fluid that occupied less place in the inlet branch. The existence of such a particle free layer near the wall has been observed for long in blood circulation. More generally, it can be due to lateral migration towards the centre, which can be of inertial origin (high Reynolds number regime) [20–24], or viscous one. In such a situation of low Reynolds number flow, while a sphere does not migrate transversally due to symmetry and linearity in the Stokes equation, deformable objects such as vesicles (closed lipid membranes) [25], red blood cells [26, 27] that exhibit similar dynamics as vesicles [28, 29], drops [30, 31] or elastic capsules [26, 27, 32], might adopt a shape that allows lateral migration. This migration is due to the presence of walls [33–35] as well as to the non-constant shear rate [36, 37]. Even in the case where no migration occurs, the initial distribution is still not homogeneous: since the barycentre of particles cannot be closer to the wall than their radius, there is always some particle free layer near the walls. This sole effect will favour the high flow rate branch.

As we want to focus in this paper on the question of cross streamline migration in the vicinity of the bifurcation, we will consider rigid spheres, for which no transverse migration in the upstream channel is expected, that are in the vanishing concentration limit and flow through a symmetric bifurcation, that is the T-shaped bifurcation shown on figure 1(b), where the two daughter branches have same cross section and are equally distributed relatively to the inlet channel.

In the literature, the most common symmetric case that is considered is the Y-shaped bifurcation with daughter branches leaving the bifurcation with a 45° angle relatively to the inlet channel, and cross sections identical as the one of the inlet channel (figure 1a) [6–11]. The T-shaped bifurcation (figure 1b) has attracted little attention [5, 38]. All studies but ref. [38] show results for rigid spherical particles, while some results for deformable particles are given in refs. [11, 38]. In all the latter papers, although the authors are sometimes conscious that the depletion and attraction effects might screen each other, the relative weight of each phenomenon is not really discussed. However, Yang *et al.* [10] consider explicitly that there must be some *attraction towards the high flow rate branch* and give some qualitative arguments for it. This opinion, initially introduced by Fung [2, 38, 39], is widely spread in the literature [15, 40, 41]. We shall come back to the underlying arguments in the following.

Explicit data on a possible attraction towards one branch are scarce as they can only be found in a recent two-dimensional simulations paper [11]. The authord presented simulation of two-dimensional spheres with $R \leq 0.67$ and two-dimensional deformable objects mimicking red blood cells in a symmetric Y-shaped bifurcation. For spheres, it is shown that there is an *attraction towards the low flow rate branch*, which increases with R. Deformable particles are also considered. However, it is not possible to discuss from their data (as, probably, from any other data) whether the cross streamline migration at the bifurcation is more important in this case or not: for deformable particles, transverse migration towards the centre occurs, due to the presence of walls and of non homogeneous shear rates. This migration will probably screen the attraction effect, at least partly, and it seems difficult to quantify the relative contribution of both effects. It appears finally that there should be some attraction towards the low flow rate branch, although the final result is an enrichment of the high flow rate branch due to the depletion effect in the inlet channel. On the other hand, if one considers the flow around an obstacle, as simulated in ref. [40], it seems that spherical particles are attracted towards the high flow rate side. Moreover, to date, no direct experimental proof of any attraction phenomenon exists. In section 3.1, we show experimentally that attraction towards the low flow rate branch takes place and confirm this through numerical simulations.
It is then necessary to discuss whether this attraction has important consequences on the final distributions in particles in the two daughter channels. This was not done explicitly in the work by Barber *et al.* [11]. It is done in section 3.2 where we discuss the relative weight of the attraction towards the low flow rate branch and the depletion effect, which have opposite consequences, by using our simulations.

Before presenting our data, we shall introduce useful notations (see figure 1(b)).

The half-width of the inlet branch is set as the length scale of the problem. The inlet channel divides into two branches of width $2a$ (the case $a = 1$ will be mainly considered here by default, unless otherwise stated), and spheres of radius $R \leq 1$ are considered. The flow rate at the inlet is noted Q_0, and Q_1 and Q_2 are the flow rates at the upper and lower outlets ($Q_0 = Q_1 + Q_2$). In the absence of particles, all the fluid particles situated initially above the line $y = y_f$ will eventually enter branch 1. This line is called the (unperturbed) fluid separating streamline. y_0 is the initial transverse position of the considered particle far before it reaches the bifurcation ($|y_0| \leq 1 - R$). N_1 and N_2 are the numbers of particles entering branches 1 and 2 by unit time, while $N_0 = N_1 + N_2$ have entered the inlet channel. The volume fractions in the branches are $\Phi_i = VN_i/Q_i$, where V is the volume of a particle.
With these notations, we can reformulate our question: if $y_0 = y_f$, does the particle experience a net force in the y direction (e. g. a pressure difference) that would push it towards one of the branches, while a fluid particle would remain on the separating streamline (by definition of y_f)? If so, for which position y_0^* does this pressure difference vanish, so that the particle follows the streamlines and eventually hits the opposite wall and reaches

an (unstable) equilibrium position? If $Q_1 \leq Q_2$ and $y_0^* < y_f$, then one will talk about *attraction towards the low flow rate branch.*
Following these notations, we have:

$$N_1 = \int_{y_0^*}^{1} n(y) u_x^*(y) dy, \tag{1}$$

$$Q_1 = \int_{y_f}^{1} u_x(y) dy, \tag{2}$$

where $n(y)$ is the mean density in particles at height y in inlet branch, u_x^* and u_x are respectively the particles and flow longitudinal upstream velocities. N_0 and Q_0 are given by the same formula with $y_0^* = y_f = -1$.
The Zweifach-Fung effect can then be written as follows: if $Q_1/Q_0 < 1/2$ (branch 1 receives less flow than branch 2) then $N_1/N_0 < Q_1/Q_0$ (branch 1 receives even less particles than fluid) or equivalently $\Phi_1 < \Phi_0$ (the particle concentration is decreased in the low flow rate branch).

2. METHOD

2.1 Experimental setup

We studied the behaviour of hard balls as a first reference system. Since the potential migration across streamlines is linked to the way the fluid acts on the particles, we also studied spherical fluid vesicles. They are closed lipid membranes enclosing a Newtonian fluid. The lipids that we used are in liquid phase at room temperature, so that the membrane is a two-dimensional fluid. In particular, it is incompressible (so that spherical vesicles will remain spherical even under stress, unlike drops), but it is easily sheared: it entails that a torque exerted by the fluid on the surface of the particle can imply a different response whether it is a solid ball or a vesicle. Moreover, since vesicle suspensions are polydisperse, it is a convenient way to vary the radius R of the studied object.
The experimental setup is a standard microfluidic chip made of polydimethylsiloxane bonded on a glass plate (figure 2). We wish to observe what happens to an object located around position y_f that is, in branch which branch it goes at the bifurcation. In order to determine the corresponding y_0^*, we need to scan different initial positions around y_f. One solution would be to let a suspension flow and hope that some of the particles will be close enough to the region of interest. In the meantime, as we shall see, the cross streamline effect is weak and requires precise measurement, and noticeable effects appear only at high radius R, typically $R > 0.5$. With such objects, clogging is unavoidable, which would modify the flow rates ratio, and if a very dilute suspension is used, it is likely that the region of interest will only partly be scanned.
Therefore we designed a microfluidic system allowing to use only one particle, that would go through the bifurcation with a controlled initial position y_0, would be taken back, its position y_0 modified, would flow again in the bifurcation, and so on. Moreover, we allowed continuous modification of the flow rate ratio between the two daughter branches. The core of the chip is the five branch crossroad shown in inset on figure 2. These five branches have different lengths and are linked to reservoirs placed at different heights, in order to induce a flow by hydrostatic pressure gradient. A focusing device (branches a,b and c) is placed before the bifurcation of interest (branches 1 and 2), in order to control the lateral position of the particle. Particles are initially located in the central branch a, where the flow is weak and the incoming particles are pinched between the two lateral flows. In order to modify the position y_0 of the particle, the relative heights of the reservoir linked to the lateral branches are modified. The total flow rate and the flow rate ratios between the two daughter branches after the bifurcation are controlled by varying the heights of the two outlet reservoirs. Note the flow rates ratio also depends on the heights of the reservoirs linked to inlet branches a, b and c. Since the two latter must be continuously modified to vary the position y_0 of the incoming particle in order to find y_0^* for a given flow rate ratio, it is convenient to place them on a pulley so that their mean height is always constant (the resistances of branches b and c being equal). If the total flow rate is a relevant parameter (which is not be the case here since we consider only Stokes flow of particles that do not deform), one can do the same with the two outlet reservoirs. In such a situation, if reservoir of branch a is placed at height 0, reservoirs of branches b and c at heights $\pm h_0$, and reservoirs of branches 1 and 2 at height $-H+h$ and $-H-h$, the flow rate ratio is governed by setting (h, H) and h_0 can be modified independently in order to control y_0. Once the particle has gone through

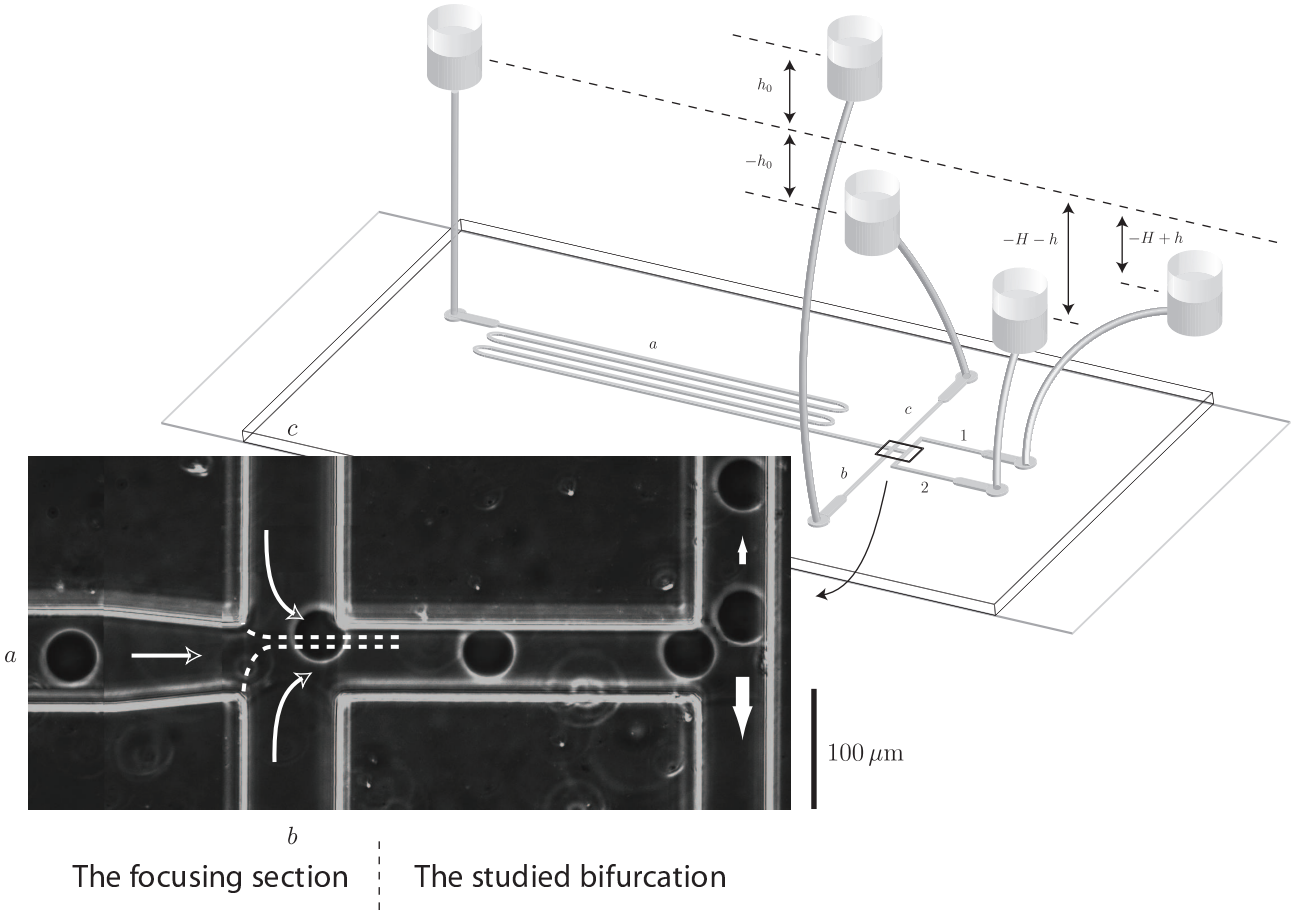

Figure 2: Scheme of the microfluidic device. The photograph shows the trajectory of a particle from branch a to branch 1 after having been focused on a given streamline thanks to flows from lateral branches b and c.

the bifurcation, height H and the height of reservoir a are modified so that the particle comes back to branch a, and h_0 is modified in order to get closer and closer to position y_0^*. Q_1/Q_0 (or, equivalently, y_f) is a function of H, h, and the flow resistances of the five branches of rectangular cross sections, which are known functions of their lengths, widths and thicknesses [42]. The accuracy of the calculation of this function was checked by measuring y_0^* for small particles, that must be equal to y_f.
Note that the length of the channel is much more important than the size of a single flowing particle, so that we can neglect the contribution of the latter in the resistance to the flow: hence, even though we control the pressures, we can consider that we work at fixed flow rates.

At the bifurcation level, channels widths are all equal to $57 \pm 0.2\mu$m. Their thickness is $81 \pm 0.3\mu$m. We used polystyrene balls of maximum radius 40.5 ± 0.3 μm in soapy water (therefore $R \leq 0.71$) and fluid vesicles of size $R \leq 0.60$. Vesicles membrane is a dioleoylphosphatidylcholine lipid bilayer enclosing an inner solution of sugar (sucrose or glucose) in water. Vesicles are produced following the standard electroformation method [43]. Maximum flow velocity at the bifurcation level was around 1 mm.s^{-1}, so that the Reynolds number Re $\simeq 10^{-1}$.

2.2 The numerical model

Our problem is a simple fluid/structure interaction one and can be modeled by Navier-Stokes equations for the fluid flow and Newton-Euler equations for the sphere. These two problems can be coupled in a simple manner:

- The action of fluid on the sphere is modeled by the hydrodynamic force and torque acting on its surface. They are used as the right hand sides of Newton-Euler equations.
- The action of the sphere on fluid can be modeled by a non-slip boundary conditions on the sphere (in the Navier-Stokes equations).

However, this explicit coupling can be unstable numerically and its resolution often requires very small time steps. In addition, as we have chosen to use finite element method **FEM** (for accuracy reasons) and since the position of the sphere evolves in time we have to remesh the computational domain at each time step or in best cases at each few time steps.
For all these reasons we chose another strategy to model our problem. Instead of using Newton-Euler equations for modeling the sphere motion and Navier-Stokes equations for the fluid flow, we use only the Stokes equations in the whole domain of the bifurcation (including the interior of the sphere). The use of Stokes equations is justified by the small Reynolds number in our case and the presence of the sphere is rendered by a second fluid with a 'huge' viscosity on which we impose a rigid body constraint. This type of strategy is widely used in the literature with different names e.g. the so called FPD (Fluid Particle Dynamics) method [44, 45]) but we can group them under the generic name of penalty-like methods. The one that we use is mainly developed by Lefebvre *et al.* [46, 47] and we can find a mathematical analysis of these types of methods in ref. [48].
In what follows we describe briefly the basic ingredients of the finite element method and penalty technique applied to our problem.
The fluid flow is governed by Stokes equations that can be written as follow:

$$-\nu\Delta\,\mathbf{u} + \nabla p = 0 \text{ in } \Omega_f, \tag{3}$$

$$\nabla \cdot \mathbf{u} = 0 \text{ in } \Omega_f, \tag{4}$$

$$\mathbf{u} = \mathbf{f} \text{ on } \partial\Omega_f. \tag{5}$$

Where:

- ν, $\mathbf{u}$ and p are respectively the viscosity, the velocity and the pressure fields of the fluid,
- Ω_f is the domain occupied by the fluid. Typically $\Omega_f = \Omega \setminus \bar{B}$ if we denote by Ω the whole bifurcation and by B the rigid particle,
- $\partial\Omega_f$ is the border of Ω_f,
- $\mathbf{f}$ is some given function for the boundary conditions.

It is known that under some reasonable assumptions the problem (3)-(4)-(5) has a unique solution $(\mathbf{u}, p) \in H^1(\Omega_f)^2 \times L^2_0(\Omega_f)$ [49]. In the sequel we will use the following functional spaces:

$$L^2(\Omega) = \{f : \Omega \to \mathbb{R}; \int_\Omega |f|^2 < +\infty\}, \tag{6}$$

$$L^2_0(\Omega) = \{f \in L^2(\Omega); \int_\Omega f = 0\}, \tag{7}$$

$$H^1(\Omega) = \{f \in L^2(\Omega); \nabla f \in L^2(\Omega)\}, \tag{8}$$

$$H^1_0(\Omega) = \{f \in H^1(\Omega); f = 0 \text{ on } \partial\Omega\}. \tag{9}$$

As we will use **FEM** for the numerical resolution of problem (3)-(4)-(5), we need to rewrite it in a variational form (an equivalent formulation of the initial problem). For sake of simplicity, we start by writing it in a standard way (fluid without sphere), then we modify it using penalty technique to take into account the presence of the particle. In what follow we describe briefly these two methods, the standard variational formulation for the Stokes problem and the penalty technique.

2.2.1 Variational formulation

Let us first recall the deformation tensor τ which will be useful in the sequel

$$\tau(\mathbf{u}) = \frac{1}{2}\left(\nabla\mathbf{u} + (\nabla\mathbf{u})^t\right). \tag{10}$$

Thanks to incompressibility constraint $\nabla \cdot \mathbf{u} = 0$ we have

$$\Delta\,\mathbf{u} = 2\nabla \cdot \tau(\mathbf{u}). \tag{11}$$

Hence, the problem (3)-(4)-(5) can be rewritten as follows: find $(\mathbf{u}, p) \in H^1(\Omega_f)^2 \times L^2_0(\Omega_f)$ such that:

$$-2\nu\nabla \cdot \tau(\mathbf{u}) + \nabla p = 0 \text{ in } \Omega_f, \tag{12}$$

$$\nabla \cdot \mathbf{u} = 0 \text{ in } \Omega_f, \tag{13}$$

$$\mathbf{u} = \mathbf{f} \text{ on } \partial\Omega_f. \tag{14}$$

By simple calculations we show that problem (12)-(13)-(14) is equivalent to this one: find $(\mathbf{u}, p) \in H^1(\Omega_f)^2 \times L^2_0(\Omega_f)$ such that:

$$2\nu \int_{\Omega_f} \tau(\mathbf{u}) : \tau(\mathbf{v}) - \int_{\Omega_f} p\nabla \cdot \mathbf{v} = 0, \forall \mathbf{v} \in H^1_0(\Omega_f)^2, \tag{15}$$

$$\int_{\Omega_f} q\nabla \cdot \mathbf{u} = 0, \forall q \in L^2_0(\Omega_f), \tag{16}$$

$$\mathbf{u} = \mathbf{f} \text{ on } \partial\Omega_f, \tag{17}$$

where : denotes the double contraction.

2.2.2 Penalty method

We chose to use the penalty strategy in the framework of **FEM** that we will describe briefly here (see [46, 47] for more details).
The first step consists in rewriting the variational formulation (15)-(16)-(17) by replacing the integrals over the real domain occupied by the fluid ($\Omega_f = \Omega \setminus \bar{B}$) by those over the whole domain Ω (including the sphere B). Which means that we extend the solution $(\mathbf{u}, p)$ to the whole domain Ω. More precisely, by the penalty method we replace the particle by an artificial fluid with huge viscosity. This is made possible by imposing a rigid body motion constraint on the fluid that replaces the sphere ($\tau(\mathbf{u}) = 0$ in B). Obviously, the divergence free constraint is also insured in B.
The problem (15)-(16)-(16) is then modified as follows: find $(\mathbf{u}, p) \in H^1(\Omega)^2 \times L^2_0(\Omega)$ such that:

$$2\nu \int_{\Omega} \tau(\mathbf{u}) : \tau(\mathbf{v}) + \frac{2}{\varepsilon} \int_B \tau(\mathbf{u}) : \tau(\mathbf{v}) - \int_{\Omega} p\nabla \cdot \mathbf{v} = 0, \forall \mathbf{v} \in H^1_0(\Omega)^2, \tag{18}$$

$$\int_{\Omega} q\nabla \cdot \mathbf{u} = 0, \forall q \in L^2_0(\Omega), \tag{19}$$

$$\mathbf{u} = \mathbf{f} \text{ on } \partial\Omega. \tag{20}$$

Where $\varepsilon \ll 1$ is a given penalty parameter.
Finally, if we denote the time discretization parameter by $t_n = n\delta t$, the velocity and the pressure at time t_n by $(\mathbf{u}_n, p_n)$, the velocity of the sphere at time t_n by $\mathbf{V}_n$ and its centre position by $\mathbf{X}_n$, we can write our algorithm as:

$$\mathbf{V}_n = \frac{1}{Volume(B)} \int_B \mathbf{u}_n \tag{21}$$

$$\mathbf{X}_{n+1} = \mathbf{X}_n + \delta t \mathbf{V}_n \tag{22}$$

$(\mathbf{u}_{n+1}, p_{n+1})$ solves:

$$2\nu \int_{\Omega} \tau(\mathbf{u}_{n+1}) : \tau(\mathbf{v}) + \frac{2}{\varepsilon} \int_B \tau(\mathbf{u}_{n+1}) : \tau(\mathbf{v}) - \int_{\Omega} p_{n+1}\nabla \cdot \mathbf{v} = 0, \forall \mathbf{v} \in H^1_0(\Omega)^2, \tag{23}$$

$$\int_{\Omega} q\nabla \cdot \mathbf{u}_{n+1} = 0, \forall q \in L^2_0(\Omega), \tag{24}$$

$$\mathbf{u}_{n+1} = \mathbf{f} \text{ on } \partial\Omega. \tag{25}$$

The implementation of algorithm (21)-(22)-(23)-(24)-(25) is done by using a user-friendly finite element software: `Freefem++` [50].
Finally, we consider the bifurcation geometry shown in figure 1(b) and impose no-slip boundary conditions on all walls and we prescribe parabolic velocity profiles at the inlets and outlets such that, for a given choice of

flow rate ratio, $Q_0 = Q_1 + Q_2$. For a given initial position y_0 of the sphere of given radius R at the outlet, the full trajectory is calculated until it definitely enters one of the daughter branches. A dichotomy algorithm is used to determine the key position y_0^*. Spheres of radius R up to 0.8 are considered.
In practice, the penalty technique may deteriorate the preconditionning of our underlying linear system. To overcome this problem, one can regularize equation (24) by replacing it with this one:

$$-\varepsilon_0 \int_\Omega p_{n+1} q + \int_\Omega q \nabla \cdot \mathbf{u}_{n+1} = 0, \forall q \in L_0^2(\Omega), \tag{26}$$

where $\varepsilon_0 \ll 1$ is a given parameter.

3. RESULTS AND DISCUSSION

3.1 The cross streamline migration

3.1.1 The particle separating streamlines

In figure 3 we show the position of the particle separating line y_0^* relatively to the position of the fluid separating line y_f when branch 1 receives less fluid than branch 2 (see figure 1b), which is the main result of this paper. For all particles considered, in the simulations or in the experiments, we find that the particle separating line lies below the fluid separating line, the upper branch being the low flow rate branch. These results clearly indicate an attraction towards the low flow rate branch: while a fluid element located below the fluid separating streamline will enter into the high flow rate branch, a solid particle can cross this streamline and enter into the low flow rate branch, providing it is not too far initially. It is also clear that the attraction increases with the sphere radius R.
In particular, in the experiments (figure 3a), particles of radius $R \lesssim 0.3$ behave like fluid particles. $R = 0.52$ balls show a slight attraction towards the low flow rate branch, while the effect is more marked for big balls of radius $R = 0.71$. Vesicles show comparable trend and it seems from our data that solid particles or vesicles with fluid membrane behave similarly in the vicinity of the bifurcation.
In the simulations (figure 3b) we see clearly that for a given R, the discrepancy between the fluid and particle behaviour increases when Q_1/Q_0 decreases. On the contrary, in the quasi-two-dimensional case of the experiments, the difference between the flow and the particle streamlines seems to be rather constant in a wide range of Q_1/Q_0 values. Finally, for small enough values of Q_1/Q_0, the attraction effect is more pronounced in the two-dimensional case than in the quasi-two-dimensional one, as shown on figure 3(a) for $R = 0.71$. This was to be expected, since this effect has something to do with the non zero size of the particle and the real particle to channel size ratio is lower in the experiments for a given R, due to the third dimension. In all cases, below a given value of Q_1/Q_0, the critical position y_0^* would enter the depletion zone $y_0 > 1 - R$, so that no particle will eventually enter the low flow rate branch. The corresponding critical Q_1/Q_0 is much lower in the two-dimensional case than in the experimental quasi-two-dimensional situation (see figure 3a).

3.1.2 Discussion

The first argument for some attraction towards one branch was initially given by Fung [2, 38, 39] and strengthened by recent simulations [51]: a sphere in the middle of the bifurcation is considered ($y_0 = 0$) and it is argued that it should go to the high flow rate branch since the pressure drop $P_0 - P_2$ is higher than $P_0 - P_1$ because $Q_2 > Q_1$ (see figure 1(b) for notations). This is true (we also found $y_0^* > 0$ when $Q_1 < Q_2$) but this is not the point to be discussed: if one wishes to discuss the increase in volume fraction in branch 2, therefore to compare the particles and fluid fluxes N_2 and Q_2, one needs to focus on particles in the vicinity of the fluid separating streamline (to see whether or not they behave like the fluid) and not in the vicinity of the middle of the channel. On the other hand, this misleading argument by Fung has led to the idea that there must be some attraction towards the high flow rate branch in the vicinity of the fluid separating streamline [10], which appears now in the literature as a well established fact [15, 41].
In ref. [11], Fung's argument is rejected, although it is not explained why. Arguments for attraction towards the low flow rate branch (that is, $P_2 > P_1$ on figure 1(b)) are given, considering particles in the vicinity of the fluid separating streamline. The authors' main idea is, first, that some pressure difference $P_0 - P_i$ builds up on each side of the particle because it goes more slowly than the fluid. Then, as the particle intercepts a relatively more important area in the low flow rate branch region ($y_f < y < 1$) than in the high flow rate region, they consider

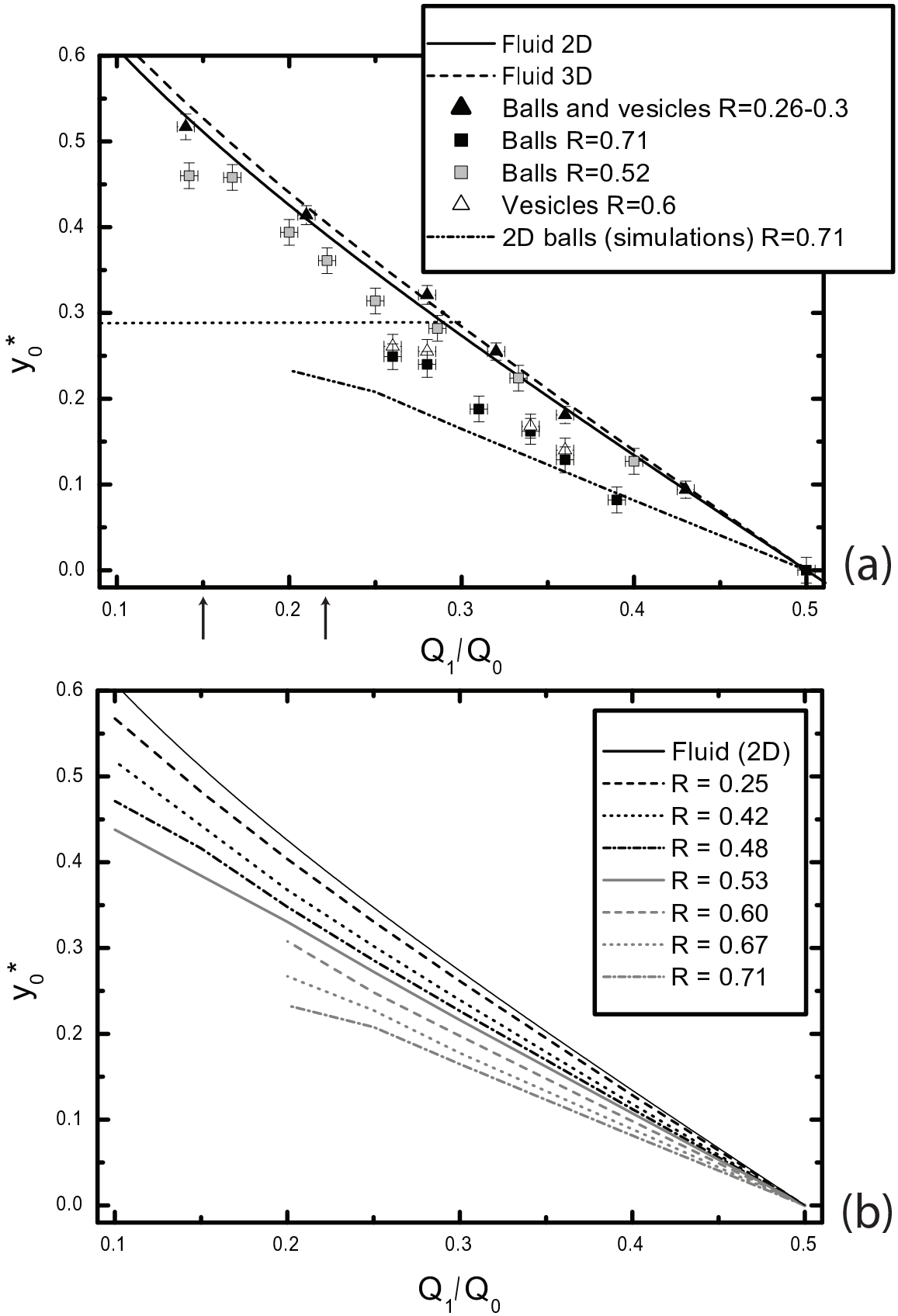

Figure 3: Position of the particle separating line y_0^*. The T-bifurcation with branches of equal widths is considered. Branch 1 receives flow from high y values, so $y_0^* < y_f$ for $Q_1/Q_0 < 1/2$ indicates attraction towards the low flow rate branch (see also figure 1b). (a) Data from quasi-two-dimensional experiments and comparison with two-dimensional case for one particle size. The horizontal dotted line shows the maximum position $y_0 = 1 - R$ for $R = 0.71$ spheres. Its intersection with the curve $y_0^*(Q_1/Q_0)$ yields the critical flow rate ratio Q_1/Q_0 below which no particle enters branch 1, the low flow rate branch. This expected critical flow rates for the two- and three-dimensional cases are shown by arrows. (b) Data from two-dimensional simulations.

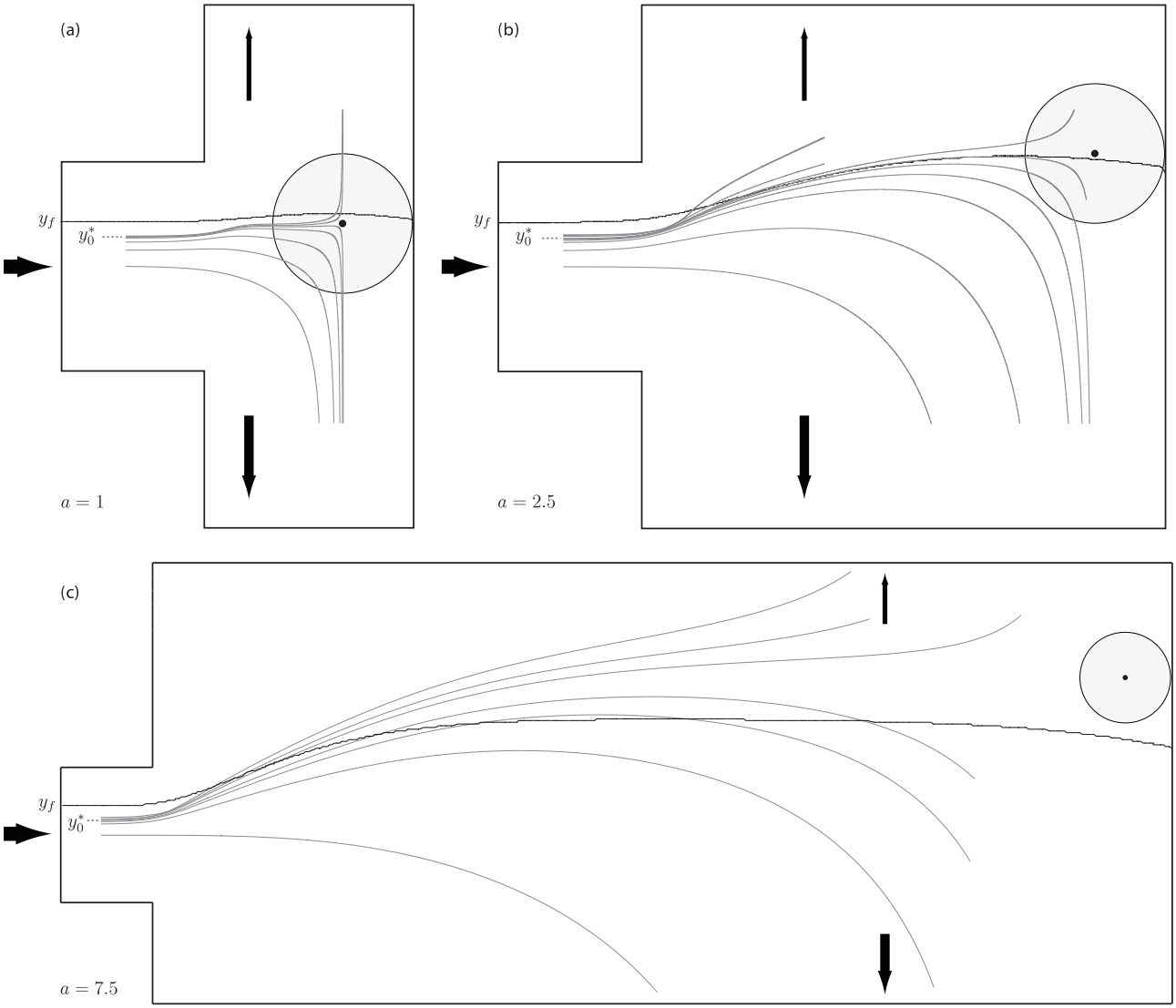

Figure 4: Grey lines: some trajectories of a $R = 0.67$ particle when $Q_1/Q_0 = 0.2$ for (a) branches of equal widths, (b) daughter branches 2.5 times wider than the inlet branch and (c) daughter branches 7.5 times wider than the inlet branch. The unperturbed fluid separating streamline starting at $y = y_f$ is shown in black. The particle is shown approximatively at its stagnation point.

that the pressure drop is more important in the low flow rate region, so that $P_2 > P_1$. The authors call this effect 'daughter vessel obstruction'.

Indeed, it is not clear in this paper where the particles must be for this argument to be valid: at the entrance of the bifurcation, in the middle of it, or close to the opposite wall as we could think since their arguments are used to explain what happens in case of daughter branches of different widths. Indeed, we shall see that the effects can be quite different according to this position and, furthermore, the notion of 'relatively larger part intercepted' is not the key phenomenon to understand the final attraction towards the low flow rate branch, even though it clearly contributes to it.

To understand this, let us focus on the simulated trajectories starting around y_0^* shown on figure 4(a) ($R = 0.67$, $Q_1/Q_0 = 0.2$). These trajectories must be analysed in comparison with the unperturbed flow streamlines, in particular the fluid separating streamline, starting at $y = y_f$ and ending up against the front wall at a stagnation point.

Particles starting around $y_0^* < y_f$ show a clear attraction towards the low flow rate branch (displacement along the y axis) as they enter the bifurcation. More precisely, there are three types of motions: for low initial position y_0 (in particular $y_0 = 0$), particles go directly into the high flow rate branch. Similarly, above y_0^*, the particles go directly into the low flow rate branch. Between some $y_0^{**} > 0$ and y_0^*, the particles first move towards the low flow rate branch, but finally enter the high flow rate branch: the initial attraction towards the low flow rate

branch becomes weaker and the particle eventually follows the streamlines entering the high flow rate branch. Note that, at this level, there is still some net attraction towards the low flow rate branch: the particle stagnation point near the opposite wall is still below the fluid separating streamline (that is, on the high flow rate side). This two-step effect is even more visible when the width $2a$ of the daughter branches is increased, so that the entrance of the bifurcation is far from the opposite wall, as shown on figures 4(b,c). The second attraction is, in such a situation, more dramatic: for $a = 7.5$, the particle stagnation point is even on the other side of the fluid separating streamline, that is, there is some attraction towards the high flow rate branch! Thus, there are clearly two antagonistic effects along the trajectory. In the first case of branches of equal widths, where the opposite wall is close to the bifurcation entrance, the second attraction towards the high flow rate branch coexists with the attraction towards the low flow rate branch and finally only diminishes it.

These two effects occur in two very different situations. At the entrance of the channel, an attraction effect must be understood in terms of streamlines crossing: does a pressure difference build up orthogonally to the main flow direction? Near the opposite wall, the flow is directed towards the branches and being attracted means flowing up- or downstream. In both cases, in order to discuss whether some pressure difference builds up or not, the main feature is that, in a two-dimensional Stokes flow between two parallel walls, the pressure difference between two points along the flow direction scales like $\Delta P \propto Q/h^3$, where Q is the flow rate and h the distance between the two walls. This scaling is sufficient to discuss in a first order approach the two effects at stake.

The second effect is the simplest one: indeed, the sphere is placed in a quasi-elongational, but asymmetric, flow. As shown on figure 5(b), around the flow stagnation point, the particle movement is basically controlled by the pressure difference $P_2' - P_1'$, than can be written $(P_0' - P_1') - (P_0' - P_2')$. Focusing on the y component of the velocity field, which becomes all the more important as a is larger than 1, we have $P_0' - P_i' \propto Q_i/(a - R)^3$. Around the flow stagnation point, the pressure difference $P_2' - P_1'$ has then the same sign as $Q_1 - Q_2$ and is thus negative, which indicates attraction towards the high flow rate branch. For wide daughter branches, when this effect is not screened by the first one, this implies that the stagnation point for particles is above the fluid separating line, as seen on figure 4(c). The argument that we use here is similar to the one introduced by Fung [10, 39] but resolves only one part of the problem. Following these authors, it can also be pointed out that the shear stress on the sphere is non zero: in a two-dimensional Poiseuille flow of width h, the shear rate near a wall scales as Q/h^2, so the net shear stress on the sphere is directed towards the high flow rate branch, making the sphere roll along the opposite wall towards this branch.
Finally, this situation is similar to the one of a flow around an obstacle, that was considered in ref. [40] as a model situation to understand what happens at the bifurcation. Indeed, the authors find that spheres are attracted towards the high velocity side of the obstacle. However, we show here that this modeling is misleading, as it neglects the first effect, which is the one which eventually governs the net effect.

This first effect leads to an attraction towards the low flow rate branch. To understand this, let us consider a sphere located in the bifurcation with transverse position $y_0 = y_f$. The exact calculation of the flow around it is much too complicated, and simplifications are needed. Just as we considered the large a case to understand the second mechanism eventually leading to attraction towards the high flow rate branch, let us consider the small a limit to understand the first effect: as soon as the ball enters the bifurcation, it hits the front wall. On each side, we can write in a first approximation that the flow rate between the sphere and the wall scales as $Q \propto \Delta P h^3$, where $\Delta P = P_0 - P_i$ is the pressure difference between the back and the front of the sphere, and h the distance between the sphere and the wall (see figure 5a).
Since the ball touches the front wall, the flow rate Q is either Q_1 or Q_2 and is, by definition of y_f, the integral of the unperturbed Poiseuille flow velocity between the wall and the $y = y_f$ line, so $Q \propto \tilde{h}^2 - \tilde{h}^3/3$, where $\tilde{h} = 1 \pm y_f$ (see figure 5(a) for notations).
We have then, on each side:

$$\Delta P \propto \frac{\tilde{h}^2 - \tilde{h}^3/3}{h^3}. \tag{27}$$

To make the things clear, let us consider then the extreme case of a flat particle: $h = \tilde{h}$. Then $\Delta P \propto 1/\tilde{h} - 1/3$ is a decreasing function of $\tilde{h}$, that is, a decreasing function of Q. Therefore, the pressure drop is more important on the low flow rate side, and finally $P_1 < P_2$: there is an attraction towards the low flow rate branch. This is exactly the opposite result from the simple view claiming that there is some attraction towards the high flow rate branch since ΔP scales as Q/h^3 so as Q. Since one has to discuss what happens for a sphere in the vicinity of

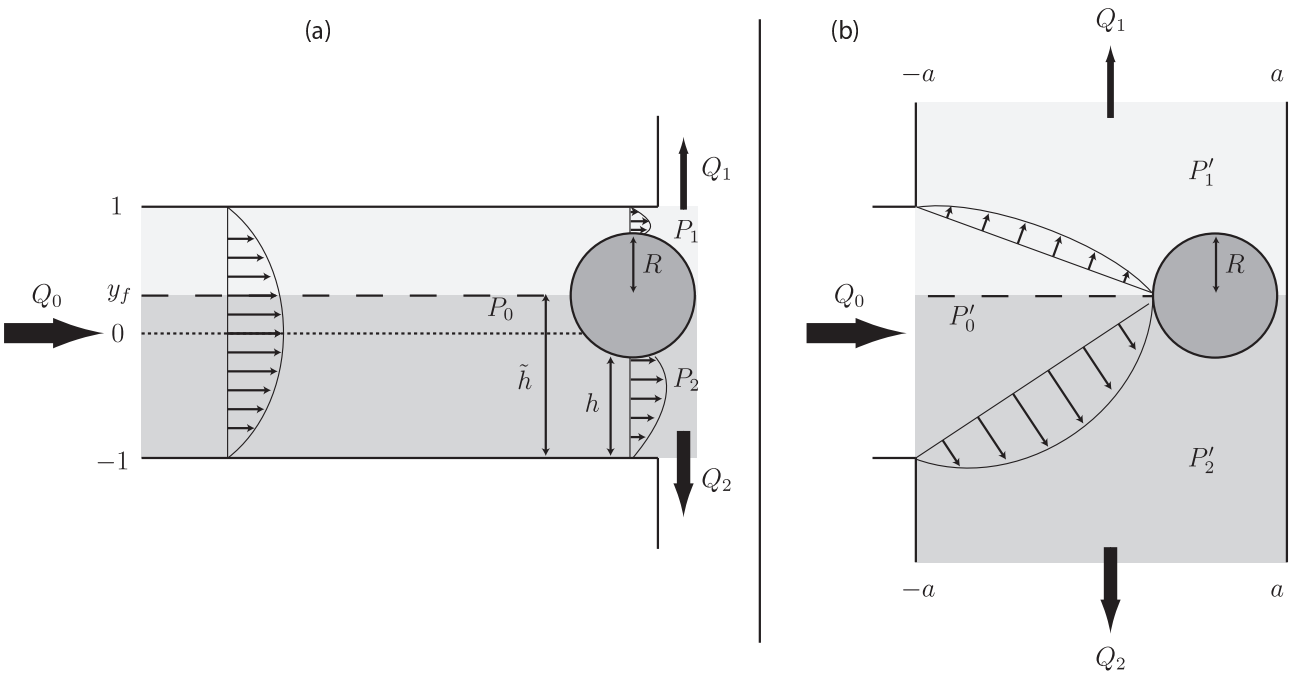

Figure 5: Scheme of the geometry considered for the two effects occurring in the bifurcation. (a) Entrance of the bifurcation: attraction towards the low flow rate branch ($P_1 < P_2$). (b) opposite wall: attraction towards the high flow rate branch ($P_1' > P_2'$).

the separating line, Q and $\tilde{h}$ are not independent. This is the key argument. Note finally that there is no need for some obstruction arguments to build up a different pressure difference on each side. It only increases the effect since the function $\tilde{h} \mapsto (\tilde{h}^2 - \tilde{h}^3/3)/(\tilde{h} - R)^3$ decreases faster than the function $\tilde{h} \mapsto (\tilde{h}^2 - \tilde{h}^3/3)/\tilde{h}^3$. One can be even more precise and take into account the variations in the gap thickness as the fluid flows between the sphere to calculate the pressure drop by lubrication theory. Still, it is found that ΔP is a decreasing function of $\tilde{h}$.

In the more realistic case $a \simeq 1$, the flow repartition becomes more complex, and the particle velocity along the x axis is not zero. Yet, as it is reaching a low velocity area (the velocity along x axis of the streamline starting at y_f drops to 0), its velocity is lower than its velocity at the same position in a straight channel. In addition, as the flow velocities between the sphere and the opposite wall are low, and since the fluid located e. g. between y_f and the top wall will eventually enter the top branch by definition, we can assume it will mainly flow between the sphere and the top wall. Note this is not true in a straight channel: there are no reasons for the fluid located between one wall and the $y = y_0$ line, where y_0 is the sphere lateral position, to enter completely, or to be the only fluid to enter, between the wall and the particle. Therefore, we can assume that the arguments proposed to explain the attraction towards the low flow rate branch remain valid, even though the net effect will be weaker. Note finally that, contrary to what discussed for the second effect, the particle rotation probably plays a minor role here, as in this geometry the shear stress exerted by the fluid on the particle will mainly result in a force acting parallel to the x axis.

Finally, this separation into two effects can be used to discuss a scenario for bifurcations with channels of different widths: if the inlet channel is broadened, the first effect becomes less strong while the second one is not modified, which results in a weaker attraction towards the low flow rate branch. If the outlet channels are broadened, as in figures 4(b,c), it becomes more subtle. Let us start again by the second effect (migration up- or downstream) before the first effect (transverse migration). As seen on figure 4, the position of the particle stagnation point (relatively to the flow separating line) is an increasing function of a, so the second effect is favoured by the broadening of the outlets: for $a \to \infty$, we end up with the problem of flow around an obstacle, while for small a, one cannot write that the width of the gap between the ball and the wall is just $a - R$, therefore independent from Q_i, as it also depends on the y position of the particle relatively to y_0'. In other words, in such a situation, the second effect is screened by the first effect. On the other hand, as a increases, the distance available for transverse migration becomes larger, which could favour the first effect, although the

R	0	0.25	0.42	0.48	0.53	0.60	0.67	0.71	0.80
α	0	-0.96	-3.45	-4.77	-6.33	-9.52	-11.6	-12.6	–
β	-1	-0.85	-0.65	-0.70	-0.64	-0.61	-0.71	-0.73	–
γ	1	0.96	0.91	0.89	0.87	0.84	0.81	0.79	0.75
ξ	–	-1.35	-1.25	-1.17	-1.09	-1.01	-0.90	-0.81	–

Table 1: Values for the fitting parameters (α, β, γ) for the longitudinal velocity $u_x^*(y_0) = \alpha y_0^4 + \beta y_0^2 + \gamma$ of a two-dimensional sphere of radius R in a Poiseuille flow of imposed velocity at infinity $u_x(y) = 1 - y^2$; for $R = 0.80$, the velocity profile is too flat to be reasonably fitted by a 3-parameter law. All velocities are equal to 0.75 ± 0.005 in the explored interval $y_0 \in [-0.15; 0.15]$. We also give the values for the fitting parameter ξ of the linear relationship between particle separating line position y_0^* and flow rate ratios: $y_0^* = \xi \times (Q_1/Q_0 - 1/2)$. For $R = 0.8$, the strong confinement leads to numerical problems as the sphere approaches the walls.

slow down of the particle at the entrance of the bifurcation becomes less pronounced.
Finally, it appears to be difficult to predict the consequences of an outlet broadening: for instance, in our two-dimensional simulations presented in figure 4 ($R = 0.67$, $Q_1/Q_0 = 0.2$), y_0^* varies from 0.27 when the outlet half-width a is equal to 1, to 0.31 when a is equal to 2.5 and drops down to 0.22 for $a = 7.5$! Note that the net effect is always an attraction towards the low flow rate branch ($y_0^* < y_f$).
For daughter branches of different widths, it was illustrated in ref. [11] that the narrower branch is favoured. This can be explained through the second effect (see figure 5b): the pressure drop $P_0' - P_i' \propto Q_i/(a - R)^3$ increases when the channel width decreases, which favours the narrower branch even in case of equal flow rates between the branches.

3.2 The consequences on the final distribution

As there is some attraction towards the low flow rate branch, we could expect some enrichment of the low flow rate branch. However, as already discussed, even in the most uniform situation, the presence of a free layer near the walls will favour the high flow rate branch. We discuss now, through our simulations, the final distribution that results from these two antagonistic effects.
In order to compute the final splitting N_1/N_0 of the incoming particles as a function of flow rate ratio Q_1/Q_0 one needs to know, according to equation (1), the position y_0^* of the particle separating line and the velocity u_x^* of the particles in the inlet channel. From figure 3 we see that y_0^* depends roughly linearly on $(Q_1/Q_0 - 1/2)$, so we will consider a linear fit of the calculated data in order to get values for all Q_1/Q_0. The longitudinal velocity u_x^* was computed for all studied particles as a function of transverse position y_0. The function $u_x^*(y_0)$ is well described by a quartic function $u_x^*(y_0) = \alpha y_0^4 + \beta y_0^2 + \gamma$, which is an approximation also used in ref. [11] (data not shown). Values for the fitting parameters for this velocity profile and for the linear relationship $y_0^* = \xi \times (Q_1/Q_0 - 1/2)$ are given in table 1.
The evolution of N_1/N_0 as a function of Q_1/Q_0 for two-dimensional rigid spheres is shown on figure 6 for two representative radii. By symmetry, considering $Q_1 < Q_2$ is sufficient. In order to discuss the enrichment in particles in the high flow rate branch (branch 2 then), it is also convenient to consider directly the volume fraction variation $\Phi_2/\Phi_0 = (N_2/Q_2)/(N_0/Q_0)$.
When $Q_1/Q_0 = 1/2$, the particles flow splits equally into the two branches: $N_1 = N_0$ and $\Phi_2 = \Phi_0$. For all explored sizes of spheres, when the flow rate in branch 1 decreases, there is an enrichment in particles in branch 2, which is precisely the Zweifach-Fung effect: $N_1/N_0 < Q_1/Q_0$ or $\Phi_2/\Phi_0 > 1$. Then, even in the most homogeneous case, the attraction towards the low flow rate branch is not strong enough to counterbalance the depletion effect that favours the high flow rate branch. However, this attraction effect cannot be considered as negligible, in particular for large particles: while, in case the particles follow their underlying fluid streamline, the maximum enrichment in the high flow rate branch would be around 40% for $R = 0.71$, it drops down to less than 17% in reality. Similarly, the critical flow rate ratio Q_1/Q_0 below which no particle enters into branch 1 is greatly shifted: from around 0.29 to around 0.15 for $R = 0.71$. For smaller spheres ($R = 0.42$), this asymmetry in the distribution between the two branches is weak: while the maximum enrichment in the high flow rate branch would be around 15% in a no-attraction case, it drops to less than 8% due to the attraction towards the low flow rate branch.
When the flow Q_1 is equal to zero or $Q_0/2$, Φ_2 is equal to Φ_0; thus there is a maximal enrichment for some

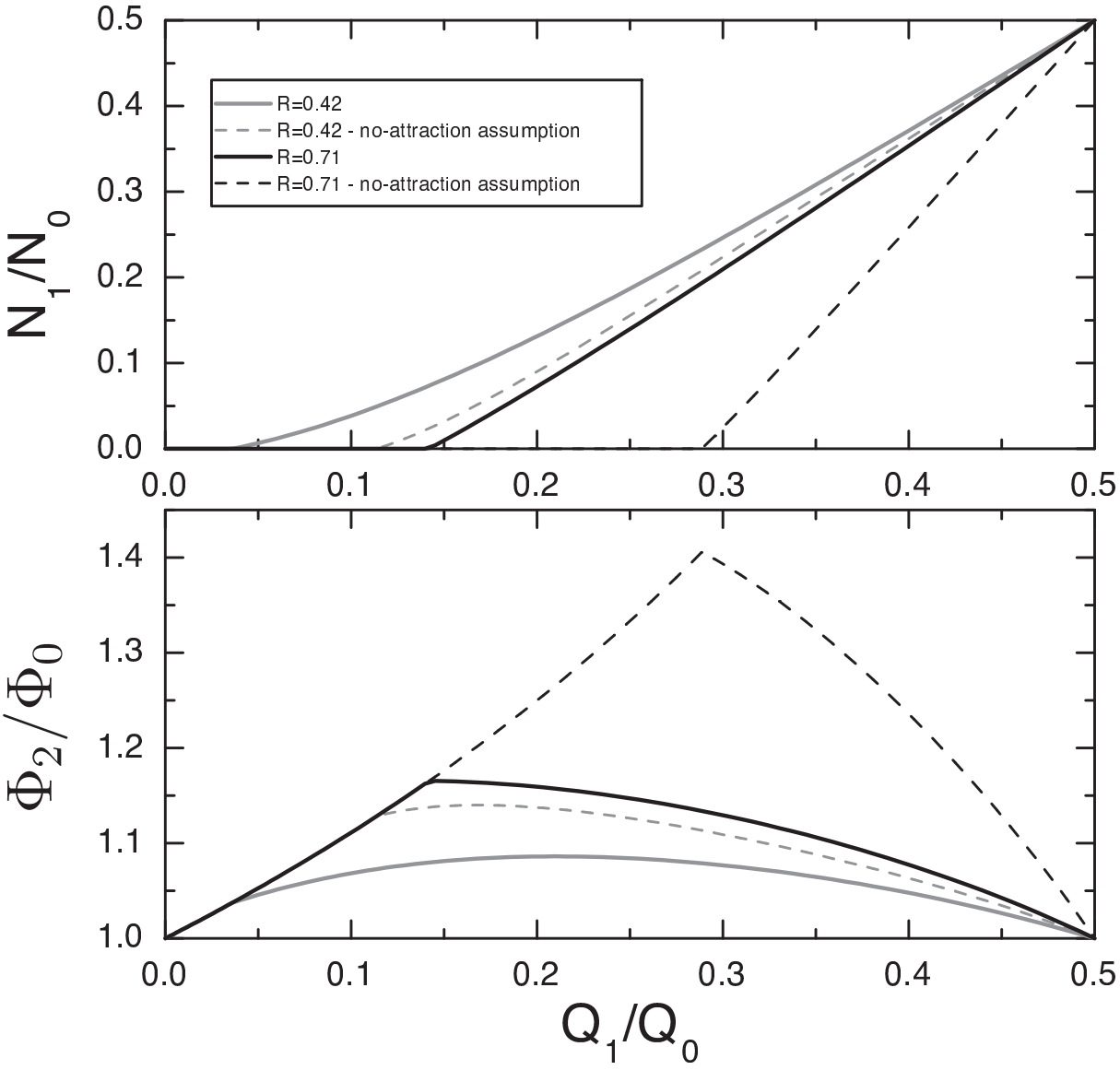

Figure 6: Full lines: spheres relative distribution N_1/N_0 and volume fraction Φ_2/Φ_0 as a function of flow rate distribution Q_1/Q_0 from our two-dimensional simulations for two representative radii $R = 0.42$ and $R = 0.71$. The curves are straightforwardly derived from equations (1) and 2 and computed values of y_0^* and u_x^* (table 1). The results are compared with the hypothesis where the particles would follow the streamlines ($y_0^* = y_f$) (dashed lines).

flow rate ratio between 0 and 1/2. The increase in Φ_2 with the decrease of Q_1 (right part of the curves of figure 6) is mainly due to the decrease of the relative importance of the free layer near the wall on the side of branch 2. Two mechanisms are responsible for the decrease of Φ_2 when Q_1 decreases (left part of the curves of figure 6): first, when no particle can enter the low flow rate branch because its hypothetical separation line y_0^* is above its maximum position $1 - R$, then the high flow rate branch receives only additional solvent when Q_1/Q_0 decreases and its particles are more diluted. Then all curves fall down on the same curve $\Phi_2/\Phi_0 = 1/(1 - Q_1/Q_0)$ corresponding to $N_1 = 0$ (or $N_2 = N_0$), which results in a sharp variation as Q_1/Q_0 goes trough the critical flow rate ratio. A smoother mechanism is also to be taken into account here, as it is finally the one that determines the maximum for smaller R. As Q_1/Q_0 decreases, branch 2 recruits fluid and particles that are closer and closer to the opposite wall. As the discrepancy between the flow and particle velocities increases near the walls, N_2 increases less than Q_2: the resulting concentration in branch 2 finally decreases.

Finally, for applicative purposes, the consequences of the attraction towards the low flow rate branch are twofold: if one wishes to obtain a particle-free fluid (e.g. plasma without red blood cells), one has to set Q_1 low enough so that $N_1 = 0$. Due to attraction towards the low flow rate branch, this critical flow rate is decreased and the efficiency of the process is lowered. If one prefers to concentrate particles, then one must find the maximum of the Φ_2/Φ_0 curve. This maximum is lowered and shifted by the attraction towards the low flow rate branch (see figure 6). Note that for small spheres (e.g. $R = 0.42$) the position of the maximum does not correspond to the point where N_1 vanishes; in addition, the shift direction of the maximum position depends on the spheres size: while it shifts to lower Q_1/Q_0 values for $R = 0.71$, it shifts to higher values for $R = 0.42$.

The choice of the geometry, within our symmetric frame, can also greatly modify the efficiency of a device. Since the depletion effect eventually governs the final distribution, narrowing the inlet channel is the first requirement. On the other hand, it also increases the attraction towards the low flow rate branch, but one can try to diminish it. As discussed in the preceding section, this can be done by widening reasonably the daughter branches. For instance, if their half-width is not 1 but 2.5, as in figure 4(b), the slope ξ in the law $y_0^* = \xi \times (Q_1/Q_0 - 1/2)$ increases by around 15% for $R = 0.67$. The critical Q_1/Q_0 below which no particle enters the low flow rate branch increases from 0.13 to 0.19, which is good for fluid-particle separation, and the maximum enrichment Φ_2/Φ_0 that can be reached is 22% instead of 15%. Alternatively, since the attraction is higher in two dimensions than in three, we can also infer that considering thicker channels, which does not modify the depletion effect, can greatly improve the final result. Note that this conclusion would have been completely different in case of high flow rate branch enrichment due to some attraction towards it, as claimed in some papers: in such a case, confining as much as possible would have been required, as it increases all kinds of cross-streamline drifts.

4. CONCLUSION

In this paper, we have focused explicitly on the existence and direction of some cross streamline drift of particles in the vicinity of a bifurcation with different flow rates in the daughter branches.
The first direct experimental proof of attraction towards the low flow rate branch was shown and arguments for this attraction were given with the help of two-dimensional simulations. In particular, we showed that this attraction is the result of two antagonistic effects: the first one, that takes place at the entrance of the bifurcation, induces migration towards the low flow rate branch, while the second one takes place near the stagnation point and induces migration towards the high flow rate branch but is not strong enough, in standard configurations of branches of comparable sizes, to counterbalance the first effect.
This second effect is the only one that was previously considered in most papers of the literature, which has lead to the misleading idea that the enrichment in particles in the high flow rate branch is due to some attraction towards it. On the contrary, it had been argued by Barber *et al.* that there should be some attraction towards the low flow rate branch. By distinguishing the two effects mentioned above, we have tried to clarify their statements.
In a second step, we have discussed the consequences of such an attraction on the final distribution of particles. It appears that the attraction is not strong enough, even in a two-dimensional system where it is stronger, to counterbalance the impact of the depletion effect. Even in the most homogeneous case where the particles are equally distributed across the channel but cannot approach the wall closer than their radius, the existence of a free layer near the walls favours the high flow rate branch, which eventually receives more particles than fluid. However, these two antagonistic phenomena are of comparable importance, and none can be neglected: the particle volume fraction increase in the high flow rate branch is typically divided by two because of the attraction effect. On the other hand, the initial distribution is a key parameter for the prediction of the final splitting. For deformable particles, initial lateral migration can induce a narrowing of their distribution, which will eventually favours the high flow rate branch. For instance, in [11], the authors had to adjust the free layer width in their simulations in order to fit experimental data on blood flow. On the other hand, in a network of bifurcations, the initially centered particles will find themselves close to one wall after the first bifurcation, which can favour a low flow rate branch in a second bifurcation.

ACKNOWLEDGEMENTS

The authors thank G. Ghigliotti for his final reading and acknowledge financial support from ANR MOSICOB and from CNES.

REFERENCES AND CITATIONS

[1] K. Svanes and B. W. Zweifach. Variations in small blood vessel hematocrits produced in hypothermic rats by micro-occlusion. *Microvasc. Res.*, 1:210–220, 1968.
[2] Y. C. Fung. Stochastic flow in capillary blood vessels. *Microvasc. Res.*, 5:34–48, 1973.
[3] A. R. Pries, T. W. Secomb, and P. Gaethgens. Biophysical aspects of blood flow in the microvasculature. *Cardiovasc. Res.*, 32:654–667, 1996.
[4] G. Bugliarello and G. C. C. Hsiao. Phase separation in suspensions flowing through bifurcations: A simplified hemodynamic model. *Science*, 143:469 – 471, 1964.
[5] S. Chien, C. D. Tvetenstrand, M. A. Epstein, and G. W. Schmid-Schonbein. Model studies on distributions of blood cells at microvascular bifurcations. *Am. J. Physiol. Heart Circ. Physiol.*, 248:H568–H576, 1985.
[6] D. M. Audet and W. L. Olbricht. The motion of model cells at capillary bifurcations. *Microvasc. Res.*, 33:377–396, 1987.
[7] R. Ditchfield and W. L. Olbricht. Effects of particle concentration on the partitioning of suspensions at small divergent bifurcations. *J. Biomech. Eng.*, 118:287–294, 1996.
[8] B. W. Roberts and W. L. Olbricht. Flow-induced particulate separations. *AIChE J.*, 49:2842–2849, 2003.
[9] B. W. Roberts and W. L. Olbricht. The distribution of freely suspended particles at microfluidic bifurcations. *AIChE J.*, 52:199–206, 2006.
[10] S. Yang, A. Ündar, and J. D. Zahn. A microfluidic device for continuous, real time blood plasma separation. *Lab on a Chip*, 6:871–880, 2006.
[11] J. O. Barber, J. P. Alberding, J. M. Restrepo, and T. W. Secomb. Simulated two-dimensional red blood cell motion, deformation, and partitioning in microvessel bifurcations. *Ann. Biomech. Eng.*, 36:1690–1698, 2008.
[12] J. W. Dellimore, M. J. Dunlop, and P. B. Canham. Ratio of cells and plasma in blood flowing past branches in small plastic channels. *Am. J. Physiol. Heart Circ. Physiol.*, 244:H635–H643, 1983.
[13] B. M. Fenton, R. T. Carr, and G. R. Cokelet. Nonuniform red cell distribution in 20 to 100 μm bifurcations. *Microvasc. Res.*, 29:103–126, 1985.
[14] R. T. Carr and L. L. Wickham. Plasma skimming in serial microvascular bifurcations. *Microvasc. Res.*, 40:179–190, 1990.
[15] R. D. Jäggi, R. Sandoz, and C. S. Effenhauser. Microfluidic depeletion of red blood cells from whole blood in high-aspect-ratio microchannels. *Microfluid Nanofluid*, 3:47–53, 2007.
[16] S. Zheng, J.-Q. Liu, and Y.-C. Tai. Streamline-based microfluidic devices for erythrocytes and leukocytes separation. *J. Microelectromech. S.*, 17:1029–1038, 2008.
[17] R. Fan, O. Vermesh, A. Srivastava, B. Yen, L. Qin, H. Ahmad, G. A. Kwong, C.-C. Liu, J. Gould, L. Hood, and J. R. Heath. Integrated barcode chips for rapid, multiplexed analysis of proteins in microliter quantities of blood. *Nat. Biotech.*, 26:1373–1378, 2008.
[18] A. R. Pries, K. Ley, M. Claassen, and P. Gaethgens. Red cell distribution at microvascular bifurcations. *Microvasc. Res.*, 38:81–101, 1989.
[19] R. Guibert, C. Fonta, and F. Plouraboue. A New Approach to Model Confined Suspensions Flows in Complex Networks: Application to Blood Flow. *Transport Porous Med.*, 83:171–194, 2010.
[20] J. A. Schonberg and E. J. Hinch. Inertial migration of a sphere in a Poiseuille flow. *J. Fluid Mech.*, 203:517–524, 1989.
[21] E. S. Asmolov. The inertial lift on a small particle in a weak-shear parabolic flow. *Phys. Fluids*, 14:15–28, 2002.
[22] S. Eloot, F. De Bisschop, and P. Verdonck. Experimental evaluation of the migration of spherical particles in three-dimensional Poiseuille flow. *Phys. Fluids*, 16:2282–2293, 2004.
[23] Y. W. Kim and J. Y. Yoo. The lateral migration of neutrally-buoyant spheres transported through square microchannels. *J. Micromech. Microeng.*, 18:065015, 2008.
[24] J. Y. Yoo and Y. W. Kim. Two-phase flow laden with spherical particles in a microcapillary. *Int. J. Mult. flow*, 36:460–466, 2010.

[25] G. Coupier, B. Kaoui, T. Podgorski, and C. Misbah. Noninertial lateral migration of vesicles in bounded Poiseuille flow. *Phys. Fluids*, 20:111702, 2008.
[26] T. W. Secomb, B. Styp-Rekowska, and A. R. Pries. Two-dimensional simulation of red blood cell deformation and lateral migration in microvessels. *Ann. Biomed. Eng.*, 35:755–765, 2007.
[27] P. Bagchi. Mesoscale simulation of blood flow in small vessels. *Biophys. J.*, 92:1858–1877, 2007.
[28] M. Abkarian, M. Faivre, and A. Viallat. Swinging of red blood cells under shear flow. *Phys. Rev. Lett.*, 98:188302, 2007.
[29] P. M. Vlahovska, T. Podgorski, and C. Misbah. Vesicles and red blood cells in flow: From individual dynamics to rheology. *C. R. Physique*, 10:775–789, 2009.
[30] S. Mortazavi and G. Tryggvason. A numerical study of the motion of drops in Poiseuille flow. part 1. lateral migration of one drop. *J. Fluid. Mech.*, 411:325–350, 2000.
[31] A. J. Griggs, A. Z. Zinchenko, and R. H. Davis. Low-Reynolds-number motion of a deformable drop between two parallel plane walls. *Int. J. Mult. Flow*, 33:182–206, 2007.
[32] F. Risso, F. Collé-Paillot, and M. Zagzoule. Experimental investigation of a bioartificial capsule flowing in a narrow tube. *J. Fluid. Mech.*, 547:149–173, 2006.
[33] P. Olla. The lift on a tank-treading ellipsoidal cell in a shear flow. *J. Phys. II France*, 7:1533–1540, 1997.
[34] M. Abkarian, C. Lartigue, and A. Viallat. Tank treading and unbinding of deformable vesicles in shear flow: Determination of the lift force. *Phys. Rev. Lett.*, 88:068103, 2002.
[35] N. Callens, C. Minetti, G. Coupier, M.-A. Mader, F. Dubois, C. Misbah, and T. Podgorski. Hydrodynamic lift of vesicles under shear flow in microgravity. *Europhys. Lett.*, 83:24002, 2008.
[36] B. Kaoui, G. Ristow, I. Cantat, C. Misbah, and W. Zimmermann. Lateral migration of a two-dimensional vesicle in unbounded Poiseuille flow. *Phys. Rev. E*, 77:021903, 2008.
[37] G. Danker, P. M. Vlahovska, and C. Misbah. Vesicles in Poiseuille flow. *Phys. Rev. Lett.*, 102:148102, 2009.
[38] R. T. Yen and Y. C. Fung. Effect of velocity distribution on red cell distribution in capillary blood vessels. *Am. J. Physiol. Heart Circ. Physiol.*, 235:H251–257, 1978.
[39] Y. C. Fung. *Biomechanics: mechanical properties of living tissues*. Springer, Berlin, 1993.
[40] A. W. El-Kareh and T. W. Secomb. A model for red blood cell motion in bifurcating microvessels. *Int. J. Multiphase Flow*, 26:1545–1564, 2000.
[41] M. Kersaudy-Kerhoas, R. Dhariwal, M. P. Y Desmulliez, and L. Jouvet. Hydrodynamic blood plasma separation in microfluidic channels. *Microfluid Nanofluid*, 8:105–114, 2010.
[42] F. M. White. *Viscous Fluid Flow*. McGraw-Hill, New-York, 1991.
[43] M. I. Angelova, S. Soleau, P. Meleard, J. F. Faucon, and P. Bothorel. Preparation of giant vesicles by external ac electric fields. kinetics and applications. *Progr. Colloid. Polym. Sci*, 89:127–131, 1992.
[44] H. Tanaka and T. Araki. Simulation method of colloidal suspensions with hydrodynamic interactions: Fluid particle dynamics. *Phys. Rev. Lett.*, 85(6):1338–1341, 2000.
[45] P. Peyla. A deformable object in a microfluidic configuration: A numerical study. *Europhys. Lett.*, 80:34001, 2007.
[46] J. Janela, A. Lefebvre, and B. Maury. A penalty method for the simulation of fluid-rigid body interaction. In *ESAIM: Proc*, volume 14, pages 115–123, 2005.
[47] A. Lefebvre. Fluid-Particle simulations with FreeFem++. In *ESAIM: Proc*, volume 18, pages 120–132, 2007.
[48] B. Maury. Numerical Analysis of a Finite Element/Volume Penalty Method. *SIAM Journal on Numerical Analysis*, 47(2):1126–1148, 2009.
[49] V. Girault and P.A. Raviart. *Finite element methods for Navier-Stokes equations: theory and algorithms*. Springer Verlag, 1986.
[50] F. Hecht and O. Pironneau. A Finite Element Software for PDEs : FreeFEM++ (`http://www.freefem.org/`), 2010.
[51] S. Yang and J. D. Zahn. Particle separation in microfluidic channels using flow rate control. In *Proceedings of IMECE04'*, 2004.